Metals **2015**, *5*, 565-577; doi:10.3390/met5020565

OPEN ACCESS

metals

ISSN 2075-4701

www.mdpi.com/journal/metals/

Article

Influence of Zr Addition on Structure and Performance of Rare Earth Mg-Based Alloys as Anodes in Ni/MH Battery

Shujun Qiu [1,2], Jianling Huang [2], Hailiang Chu [1,2,*], Yongjin Zou [1,2], Cuili Xiang [1,2], Huanzhi Zhang [1,2], Fen Xu [1,2], Lixian Sun [1,2,*], Liuzhang Ouyang [3] and Huaiying Zhou [1,2]

[1] Guangxi Key Laboratory of Information Materials, Guilin University of Electronic Technology, Guilin 541004, China; E-Mails: qiushujun@guet.edu.cn (S.Q.); zouy@guet.edu.cn (Y.Z.); xiangcuili@guet.edu.cn (C.X.); zhanghuanzhi@dicp.ac.cn (H.Z.); xufen@lnnu.edu.cn (F.X.); zhy@guet.edu.cn (H.Z.)

[2] School of Materials Science and Engineering, Guilin University of Electronic Technology, Guilin 541004, China; E-Mail: jianlinghuang@126.com

[3] School of Materials Science and Engineering, South China University of Technology, Guangzhou 510641, China; E-Mail: meouyang@scut.edu.cn

***** Authors to whom correspondence should be addressed; E-Mails: chuhailiang@guet.edu.cn (H.C.); sunlx@guet.edu.cn (L.S.); Tel.: +86-773-221-6607 (H.C.); Fax: +86-773-229-0129 (H.C.).

Academic Editor: Hugo F. Lopez

Received: 18 February 2015 / Accepted: 1 April 2015 / Published: 8 April 2015

Abstract: In this study, the substitution of Mg with Zr in $La_{0.7}Mg_{0.3}(Ni_{0.85}Co_{0.15})_{3.5}$ was carried out with the purpose of improving the electrochemical performances. The structural and hydrogen storage properties in both gas-solid reaction and the electrochemical system were systematically studied on $La_{0.7}(Mg_{0.3-x}Zr_x)(Ni_{0.85}Co_{0.15})_{3.5}$ (x = 0.05, 0.1, 0.2, 0.3) alloys. Each tested alloy is composed of $LaNi_3$ phase, $LaNi_5$ phase and $ZrNi_3$ phase with different phase abundances. The electrochemical studies indicated that all Zr-substituted anodes possessed a much higher cycling capacity retention than pristine $La_{0.7}Mg_{0.3}(Ni_{0.85}Co_{0.15})_{3.5}$. However, the maximum discharge capacity was reduced with the increase of Zr content. The potential-step tests showed that the diffusion of hydrogen atoms inside the anodes was decelerated after the introduction of Zr.

Keywords: hydrogen storage; rare earth Mg-based alloy; Ni/MH battery; elemental substitution; electrochemical performance

---

1. Introduction

Nowadays Ni/MH rechargeable batteries are employed diffusely in all kinds of portable electronic products because of longer working life and less environmental pollution [1,2]. Many classes of alloys have been used as anodes in Ni/MH batteries in past decades. At the very beginning, the first case was AB_5-type alloys contained rare earth elements [3]. However, the lower theoretical discharge capacity impedes their practical application. Subsequently, Zr-based or Ti-based alloys [4], V-based solid solution alloys [5] and Mg-based amorphous alloys [6,7] were extensively studied. However, Ti-based or Zr-based anodes need too many charge/discharge cycles to achieve their maximum discharge capacities, while Mg-based anodes quickly lose their discharge capacities because of the corrosion of Mg in KOH electrolyte [8–11].

In 2000, a newly developed alloys with the chemical composition of RMg_2Ni_9 (R represents Ca or rare earth elements) were reported by Kadir *et al.* [10–13], among which $(La_{0.65}Ca_{0.35})(Mg_{1.32}Ca_{0.68})Ni_9$ had a relatively high capacity of 1.87 wt% H_2 in gas-solid system at 283 K under 3.30 MPa H_2 pressure. Chen and coworkers demonstrated that a much higher discharge capacity of 356 mAh/g was achieved for $LaCaMgNi_9$ alloy [8]. For the case of nonstoichiometric La–Mg–Ni–Co-type alloys, the discharge capacity could reach to an extremely high value of 410 mAh/g for $La_{0.7}Mg_{0.3}Ni_{2.8}Co_{0.5}$ alloy with the comparatively good cycle durability during the initial 30 cycles [14]. Furthermore, the partial substitution of Ni with Mn or Al could give rise to an enhancement of the electrochemical properties [15–17]. Although the overall electrochemical properties are improved to some extent in the aforementioned literatures, the charge/discharge cyclic stability and the high-rate dischargeability (*HRD*) of anodes are urgently requiring further improvement. In general, the elemental substitution to form multi-component alloy is perceived as a very accessible method to enhance the electrochemical performances [18–20]. Metallic Zr, as an element for absorbing hydrogen, tends to form an oxide passive film insoluble in 6 M KOH electrolyte, which prevents further corrosion of anodes [21]. This was evidenced in Mg-based alloys, in which the introduction of Zr could result in a remarkable amelioration of the cyclic life [21] and maximum discharge capacity [22].

In this paper, Zr was selected as a partially substituting element for Mg with the purpose of the performance enhancement of La–Mg–Ni–Co-type alloys as anodes in Ni/MH battery. The structural and hydrogen storage properties in both the electrochemical system and gas-solid reaction of $La_{0.7}(Mg_{0.3-x}Zr_x)(Ni_{0.85}Co_{0.15})_{3.5}$ (x = 0.05–0.3) alloys were systematically studied.

2. Experimental Section

2.1. Materials Preparation

The purity of all raw materials is above 99%. Under argon atmosphere, $La_{0.7}(Mg_{0.3-x}Zr_x)(Ni_{0.85}Co_{0.15})_{3.5}$ (x = 0.05, 0.1, 0.2, 0.3) hydrogen storage alloys were prepared by magnetic levitation melting in a water-cooled copper crucible. To obtain homogeneous samples, the ingots were turned over and melted again for three times. Then, the ingots were mechanically crushed and ground into the powder using a mortar and pestle. The global chemical composition of each alloy was measured on an ICP–OES (Optima 8000, Perkin Elmer Inc., Waltham, MA, USA).

2.2. Materials Characterization

The phase structure was characterized on a PANalytical X'pert diffractometer with Cu K_α radiation. The diffraction patterns were analyzed using Topas software [23]. P–C isotherms were determined by a conventional Sievert-type apparatus. The activation was performed at 303 K under 3 MPa H_2 pressure. The following dehydrogenation was carried out at 573 K under dynamic vacuum for 3 h. After repeated three cycles, P–C isotherms were carried out at 303 K.

2.3. Electrochemical Tests

Each tested anode was fabricated through homogenously mixing alloy powder with Ni powder. The mixture was then pressed into a pellet with a diameter of 10 mm under a pressure of 30 MPa. Each side of the anode pellet was coated with a rounded foam nickel sheet of about 25 mm in a diameter, then pressed at 6 MPa and tightly spot-welded at the edge of foam nickel. A nickel lead wire was attached to this pressed foam nickel sheet by spot welding. The electrochemical measurements were performed in a standard open trielectrode electrolysis cell comprising a working anode of alloy pellet studied, a sintered $Ni(OH)_2$/NiOOH counter electrode, and a Hg/HgO reference electrode immersed in 6 M KOH electrolyte. High-rate dischargeability (*HRD*) and charge/discharge cycles were tested on an automatic instrument (LAND). The anodes were charged for 3 h at a current density of 300 mAh/g, rested for 5 min and then discharged to the cut-off potential of −0.6 V *versus* Hg/HgO reference electrode at a current density of 100 mAh/g. To determine the high rate dischargeability of the alloy anodes, the discharge capacities at different discharge current density were measured. The other electrochemical measurements including linear polarization (LP), electrochemical impedance spectroscopy (EIS), anodic polarization (AP) and potential-step were conducted on a Zahner Elektrik IM6e electrochemical workstation. AP and LP were measured by scanning the anode potential at a rate of 0.1 mV/s from −5 to 5 mV (*versus* open circuit potential) and 5 mV/s from 0 to 600 mV (*versus* open circuit potential) at 50% depth of discharge (DOD), respectively. EIS was conducted from 10 kHz to 5 mHz with an amplitude of 5 mV *versus* open circuit potential at 50% DOD. Before EIS tests, the anodes were fully activated by charge-discharge for three cycles.

3. Results and Discussion

XRD patterns for $La_{0.7}(Mg_{0.3-x}Zr_x)(Ni_{0.85}Co_{0.15})_{3.5}$ alloys were shown in Figure 1. Each alloy is composed of $LaNi_3$ phase and $LaNi_5$ phase except for a residual phase of $ZrNi_3$. The detailed information for crystal structure including phase composition, phase abundance, cell constants, and cell volume are summarized in Table 1. The solubility of Zr in $LaNi_5$ phase is very limited [24] and can be seen from the negligible change in the cell volume of $LaNi_5$ phase (Table 1). However, Zr must participate in $LaNi_3$ phase which is obviously from the enlarged unit cell of $LaNi_3$ phase due to Zr partially replacement of the smaller Mg and/or entrance into the Ni-site from x = 0.05 to 0.3. With Zr content increasing from 0.05 to 0.3, the phase abundance of $LaNi_3$ increases, while the phase abundance of $LaNi_5$ decreases. This indicates that the introduction of Zr into alloys facilitates the formation of $LaNi_3$ phase, which is different from the gradual substitution of La with Zr in La–Mg–Ni-type alloys [25]. It is noted that the phase abundance of non-hydrogen-absorbing phase

($ZrNi_3$) increases with x increasing. Therefore, such a variation of phase abundance will give rise to some effects on the electrochemical properties and gaseous hydrogen storage of $La_{0.7}(Mg_{0.3-x}Zr_x)(Ni_{0.85}Co_{0.15})_{3.5}$ alloys.

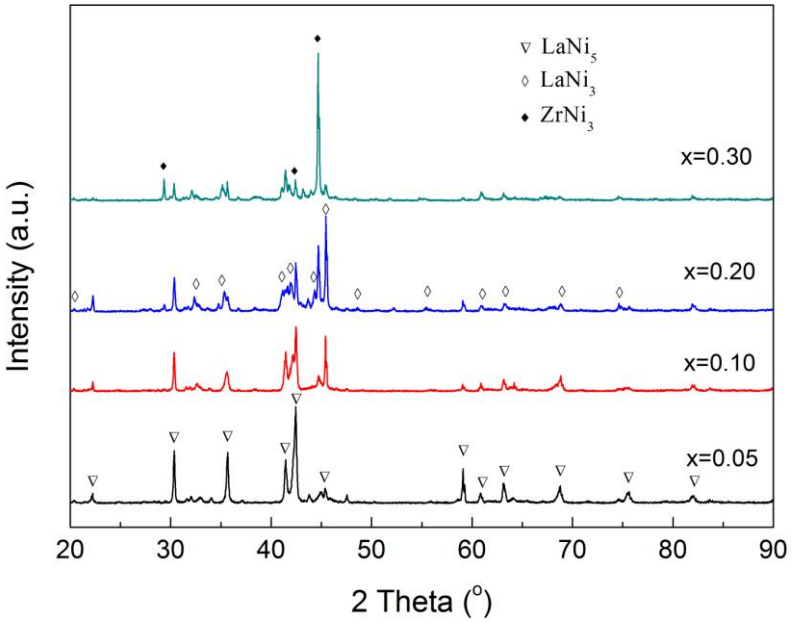

Figure 1. XRD patterns of $La_{0.7}(Mg_{0.3-x}Zr_x)(Ni_{0.85}Co_{0.15})_{3.5}$ alloys.

Table 1. The detailed structural information of $La_{0.7}(Mg_{0.3-x}Zr_x)(Ni_{0.85}Co_{0.15})_{3.5}$ alloys.

Samples	Phases	Space group (no.)	Phase abundance (wt%)	Lattice parameters (Å)		Cell volume (Å^3)	Parameters of fit
				a	*c*		
x = 0.05	$LaNi_5$	P6/mmm (191)	65.5	5.0301(5)	3.9906(5)	87.44(2)	R_{wp} = 2.7; R_p = 2.9
	$LaNi_3$	R-3m (166)	24.1	5.0388(1)	24.391(1)	536.3(3)	
	$ZrNi_3$	$P6_3/mmc$ (194)	10.4	5.2805(3)	4.2780(3)	103.3(1)	
x = 0.1	$LaNi_5$	P6/mmm (191)	49.1	5.0255(6)	3.9862(5)	87.19(2)	R_{wp} = 3.0; R_p = 3.4
	$LaNi_3$	R-3m (166)	35.3	5.0484(1)	24.601(1)	543.0(3)	
	$ZrNi_3$	$P6_3/mmc$ (194)	15.6	5.3003(4)	4.2805(6)	104.1(2)	
x = 0.2	$LaNi_5$	P6/mmm (191)	33.2	5.0232(6)	3.9832(4)	87.04(2)	R_{wp} = 4.8; R_p = 5.0
	$LaNi_3$	R-3m (166)	40.6	5.0645(2)	24.824(1)	551.4(5)	
	$ZrNi_3$	$P6_3/mmc$ (194)	26.2	5.3166(3)	4.2858(6)	104.9(20)	
x = 0.3	$LaNi_5$	P6/mmm (191)	23.5	5.0300(1)	3.9872(8)	87.36(4)	R_{wp} = 3.9; R_p = 4.3
	$LaNi_3$	R-3m (166)	47.8	5.0797(2)	25.087(1)	560.6(4)	
	$ZrNi_3$	$P6_3/mmc$ (194)	28.7	5.4320(1)	3.9806(1)	101.7(5)	

To understand the hydrogen storage properties of $La_{0.7}(Mg_{0.3-x}Zr_x)(Ni_{0.85}Co_{0.15})_{3.5}$ alloys in gas-solid system, P–C isotherms were conducted through a Sieverts' method [26] at 303 K. As shown in Figure 2, the plateau pressure clearly increases while the absorbed hydrogen capacity decreases from 1.51 (x = 0.05) to 1.02 wt% (x = 0.3), which is related to the gradual increase of the amount for non-hydrogen-absorbing $ZrNi_3$ in the alloys.

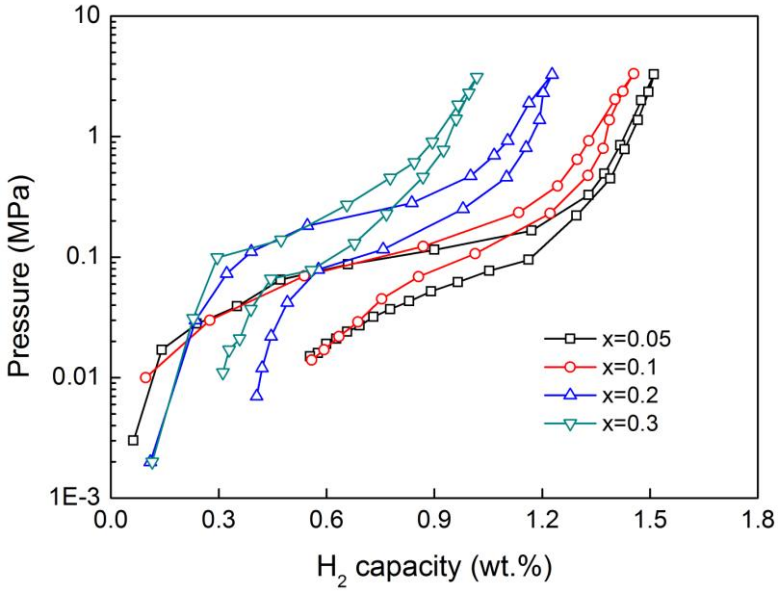

Figure 2. P–C isotherms of $La_{0.7}(Mg_{0.3-x}Zr_x)(Ni_{0.85}Co_{0.15})_{3.5}$ alloys.

Figure 3 shows charge/discharge cyclic life for $La_{0.7}(Mg_{0.3-x}Zr_x)(Ni_{0.85}Co_{0.15})_{3.5}$ anodes, and Table 2 lists their detailed electrochemical properties. All anodes could achieve their maximum discharge capacities (denoted as C_{max}) within three cycles, indicating that they can be easily activated. The C_{max} is reduced from 341.1 (x = 0.05) to 176.4 mAh/g (x = 0.3), which agrees well with the results obtained from P–C isotherms. Two factors may be responsible for this variation. First, LaMg-rich particles in the alloys serve as preferred sites for absorbing hydrogen, which is beneficial to the improvement of the discharge capacity [27]. As Mg content in the alloy is reduced by increasing substitution with Zr, the number of LaMg-rich particles is reduced, which gives rise to the gradual decrease of the discharge capacity. Second, the increasing amount of non-hydrogen-absorbing $ZrNi_3$ could also result in the reduction of the discharge capacity. Figure 4 indicates that the capacities in both gas-solid hydrogen storage and the electrochemical reaction have similar reduction with increasing abundance of $ZrNi_3$ phase. However, the cyclic stability is gradually improved with increasing content of Zr. For instance, the capacity retention after 60 cycles (denoted as C_{60}/C_{max}) increases from 53.9% (x = 0.05) to 60.8% (x = 0.2), then reduces to 58.4% (x = 0.3). Note that C_{60}/C_{max} of all anodes with Zr-substitution in our study is higher than that of Zr-free anode (C_{60}/C_{max} = 45.9%) [28]. In addition, C_{100}/C_{max} is still kept at 40.3% for anode with x = 0.1. As we all know, the capacity fading is mainly resulting from the particle pulverization upon cycling and the surface oxidation and/or corrosion of Mg, Ni and La elements [29]. In the La–Mg–Ni system, Mg and Ni were involved in a mixed hydroxide of (Mg, Ni)$(OH)_2$ and La transformed into nanoporous $La(OH)_3$ needles [30]. The cycling improvement in this study could be related to the fact that the extent of oxidation/corrosion of Mg and La is reduced because ZrO_2 was formed as a passive film on anode surface. As Zr content increases, the thickness of formed ZrO_2 film gradually increases at x = 0.05–0.2, which prevents the corrosion/oxidation of La and Mg and thus gives rise to an improvement of cyclic stability [25]. Similar improvements are observed in Zr-substituted Mg-based [21] and Ti-based anodes [31].

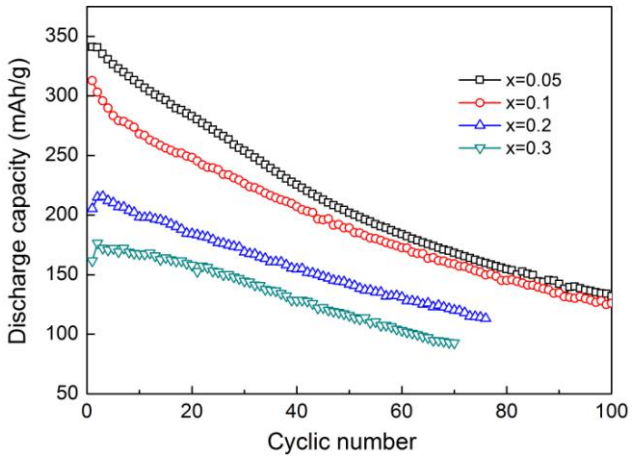

Figure 3. Cyclic life curves of $La_{0.7}(Mg_{0.3-x}Zr_x)(Ni_{0.85}Co_{0.15})_{3.5}$ anodes.

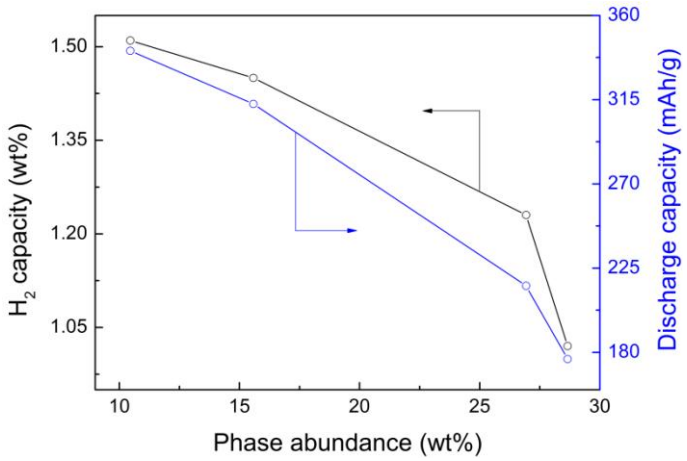

Figure 4. Relationship between hydrogen capacity (discharge capacity) and phase abundance of $ZrNi_3$.

Table 2. The electrochemical and gaseous hydrogen storage properties of $La_{0.7}(Mg_{0.3-x}Zr_x)(Ni_{0.85}Co_{0.15})_{3.5}$ alloys.

Samples	H_2 (wt.%)	C_{max} (mAh/g)	N_a	C_{60}/C_{max} (%)	HRD_{800} (%)
x = 0.05	1.51 ± 0.02	341.1 ± 0.5	1	53.9 ± 0.5	94.2 ± 0.8
x = 0.1	1.45 ± 0.01	312.8 ± 0.8	1	55.2 ± 0.3	90.6 ± 0.6
x = 0.2	1.23 ± 0.03	215.5 ± 0.6	3	60.8 ± 0.6	82.5 ± 0.3
x = 0.3	1.02 ± 0.03	176.4 ± 0.4	2	58.4 ± 0.7	78.9 ± 0.4

Figure 5 shows *HRD* of $La_{0.7}(Mg_{0.3-x}Zr_x)(Ni_{0.85}Co_{0.15})_{3.5}$ anodes at several higher discharge current densities. At 800 mA/g, *HRD* is reduced from 94.2% (x = 0.05) to 78.9% (x = 0.3). As a rule of thumb, *HRD* is an important parameter for Ni/MH batteries, which is principally determined by the anode reaction kinetics. The detailed kinetic properties can be jointly described using the exchange current density I_0, the limiting current density I_L, and the hydrogen diffusion coefficient D, which will be discussed in the forthcoming sections.

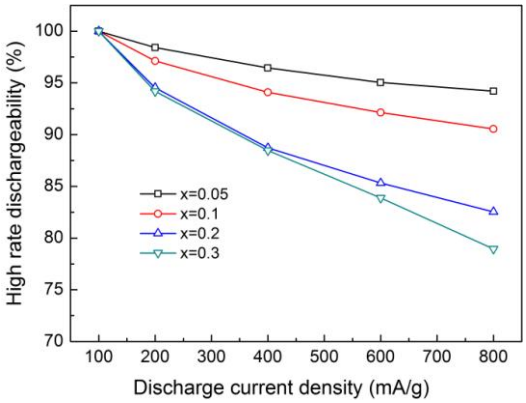

Figure 5. High-rate dischargeability (*HRD*) of $La_{0.7}(Mg_{0.3-x}Zr_x)(Ni_{0.85}Co_{0.15})_{3.5}$ anodes.

Figure 6 shows EIS of $La_{0.7}(Mg_{0.3-x}Zr_x)(Ni_{0.85}Co_{0.15})_{3.5}$ anodes. Each EIS is comprised of a tilted line and two semicircles. Based on Kuriyama's interpretation analyzed by an equivalent circuit (see the inset in Figure 6), the middle-frequency semicircle was ascribed to charge-transfer resistance [32]. Clearly shown in Figure 6, the radius of the middle-frequency semicircle is first increased to x = 0.2 and then remarkably reduced at x = 0.3, which demonstrates that the charge-transfer reaction resistance has the same variation trend. It was reported that a thicker passive film on anode surface gives rise to a higher charge-transfer reaction resistance [21]. In the present work, with the increase of Zr content, the passive film is gradually thickening, which blocks the charge-transfer reaction when x increases to x = 0.2. For the case of x = 0.3, Mg was completely substituted by Zr, the charge-transfer resistance is reduced to a certain extent, which can be related to the absence of MgO and/or $Mg(OH)_2$. As a consequence, the thickness of passive film is reduced at x = 0.3 and thus the charge-transfer reaction is facilitated.

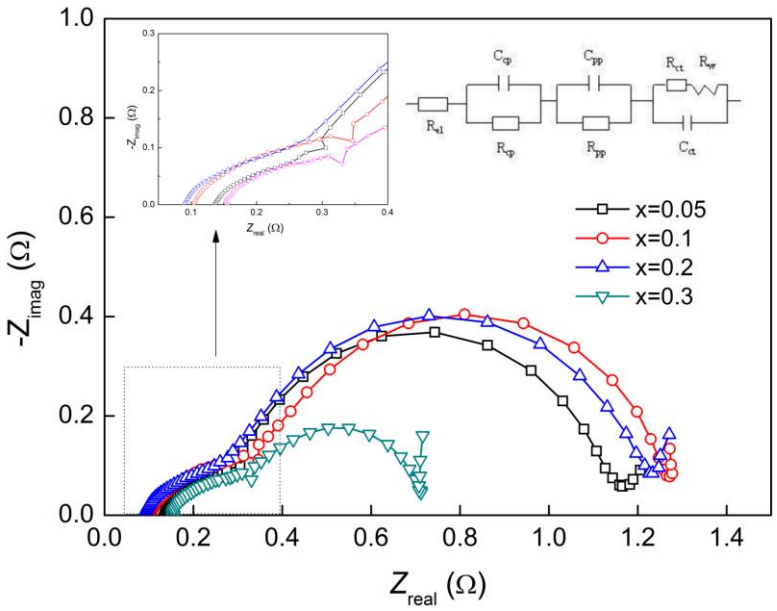

Figure 6. Electrochemical impedance spectroscopy (EIS) of $La_{0.7}(Mg_{0.3-x}Zr_x)(Ni_{0.85}Co_{0.15})_{3.5}$ anodes. The insets show the enlargement of EIS in high-frequency region and an equivalent circuit.

Table 3. Several parameters related to the anode reaction kinetics of $La_{0.7}(Mg_{0.3-x}Zr_x)(Ni_{0.85}Co_{0.15})_{3.5}$ alloys.

Samples	Polarization resistance, R_p (mΩ)	Exchange current density, I_0 (mA/g)	Limiting current density, I_L (mA/g)	Hydrogen diffusion coefficient, D (cm^2/s)
x = 0.05	132.9 ± 1.0	196.5 ± 0.6	3432.1 ± 8.1	(2.85 ± 0.04) × 10^{-10}
x = 0.1	141.7 ± 0.8	184.3 ± 0.8	2871.1 ± 5.4	(2.62 ± 0.02) × 10^{-10}
x = 0.2	148.7 ± 0.4	175.6 ± 0.7	2802.4 ± 3.4	(2.60 ± 0.01) × 10^{-10}
x = 0.3	80.4 ± 0.7	324.7 ± 0.9	2489.4 ± 9.4	(2.39 ± 0.03) × 10^{-10}

For the anode reaction kinetics, I_0 is another important parameter [33,34], which can be determined from polarization resistance R_p. R_p could be determined from LP curve shown in Figure 7 and are summarized in Table 3. R_p increases first from 132.9 (x = 0.05) to 148.7 mΩ (x = 0.2) and then reduces to 80.4 mΩ (x = 0.3). Its variation is in line with charge-transfer resistance from EIS. Based on R_p, I_0 can be calculated through the Equation (1) [34]:

$$I_0 = \frac{RT}{FR_p} \quad (1)$$

in which R, F, and T are gas constant, Faraday constant and absolute temperature, respectively. Its variation with x increasing indicates that the anode reaction kinetics is first retarded and then improved due to the reduction of the active sites resulting from a gradually thickening of the passive film. For x = 0.3, I_0 increases to a certain extent, which may be due to the reduction of passive film resulting from the absence of MgO and/or $Mg(OH)_2$ on Mg-free anode surface.

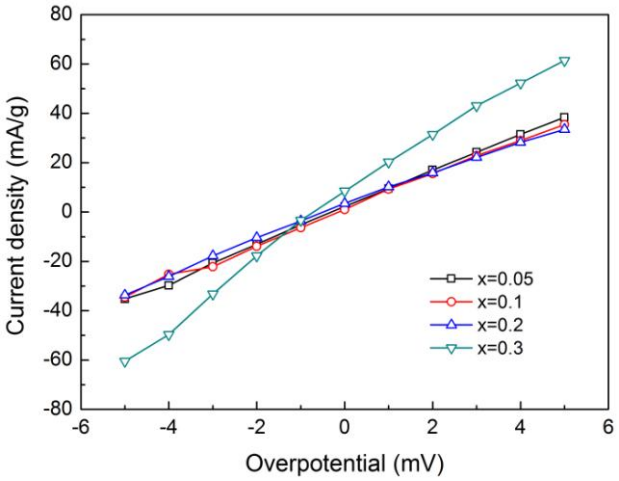

Figure 7. Linear polarization curves of $La_{0.7}(Mg_{0.3-x}Zr_x)(Ni_{0.85}Co_{0.15})_{3.5}$ anodes.

Figure 8 shows the anodic polarization (AP) curves. For each AP curve, with the increase of overpotential, there is a maximum for the anodic current density, denoted as limiting current density I_L, indicating an oxidation reaction occurring on anode surface and a resistance of further penetration for hydrogen atoms by generated oxidation products [35]. Therefore, I_L can be related to hydrogen diffusion inside anodes and the resistance on anode surface [33]. I_L decreases from 3432.1 (x = 0.05) to 2489.4 (x = 0.3), suggesting that the hydrogen diffusion is decelerated.

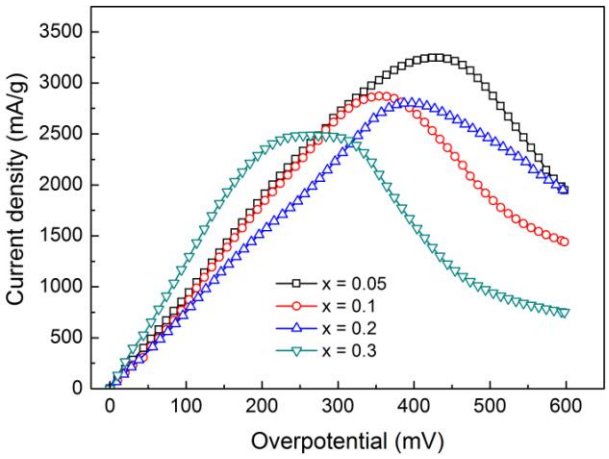

Figure 8. Anodic polarization curves of $La_{0.7}(Mg_{0.3-x}Zr_x)(Ni_{0.85}Co_{0.15})_{3.5}$ anodes.

Figure 9 shows the discharging curves at a constant potential. Each curve of semilograrithmic plot has two regions during the tested time [36]. In the beginning of each curve, the current is quickly reduced because of a rapid hydrogen depletion in electro-oxidation. For the case of the latter region, the current shows a slow and linear decrease due to hydrogen diffusion as a rate-determining step. Under this circumstance, hydrogen is provided inside the anodes based on the hydrogen concentration. Modeled as the finite hydrogen diffusion [34], *D* could be calculated using the fitted slope of the linear part through the Equation (2) [37]:

$$\log i = \log\left(\frac{6FD}{da^2}\left(C_0 - C_s\right)\right) - \frac{\pi^2}{2.303}\frac{D}{a^2}t \quad (2)$$

where *i*, *D*, *d*, *a*, C_0, C_s, and *t* represent the diffusion current density (A/g), the hydrogen diffusion coefficient (cm^2/s), the alloy density (g/cm^3), the alloy particle radius (cm), the initial hydrogen concentration (mol/cm^3), the surface hydrogen concentration (mol/cm^3), and the discharge time (s), respectively. Using the alloy particle radius of 25 μm roughly determined by sieving, *D* is calculated and also summarized in Table 3. *D* is monotonously reduced from 2.85×10^{-10} to 2.39×10^{-10} cm^2/s, in line with the results from AP curves.

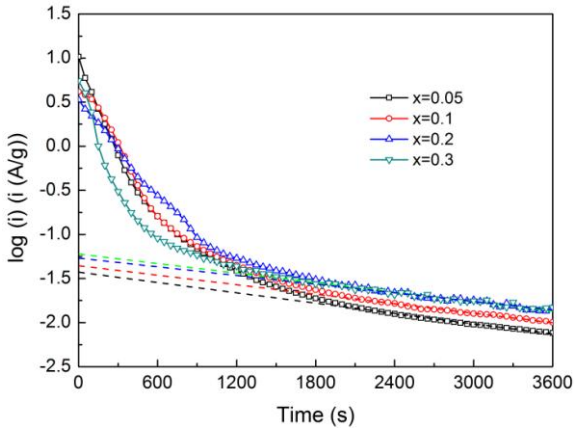

Figure 9. Semilogarithmic curves of discharge curves of $La_{0.7}(Mg_{0.3-x}Zr_x)(Ni_{0.85}Co_{0.15})_{3.5}$ anodes.

4. Conclusions

The structure and hydrogen storage properties in both gas-solid reaction and the electrochemical system of $La_{0.7}(Mg_{0.3-x}Zr_x)(Ni_{0.85}Co_{0.15})_{3.5}$ alloys were systemically investigated. XRD patterns show that all studied alloys are composed of $LaNi_3$ phase, $LaNi_5$ phase and $ZrNi_3$ residual phase. The electrochemical tests indicate that C_{60}/C_{max} first increases from 53.9% (x = 0.05) to 60.8% (x = 0.2), then reduces to 58.4% (x = 0.3) and that C_{max} is reduced from 341.1 (x = 0.05) to 176.4 mAh/g (x = 0.3), consistent with the capacities obtained from P–C isotherms in gas-solid system. The electrochemical tests such as EIS, LP and AP indicate that the Zr substitution for Mg retards the anode reaction kinetics. Furthermore, D is gradually reduced from 2.85×10^{-10} to 2.39×10^{-10} cm^2/s with the increase of Zr content.

Acknowledgments

This research was jointly sponsored by Guangxi Key Laboratory of Information Materials (Guilin University of Electronic Technology), P.R. China (Project No. 1210908–03–K), National Natural Science Foundation of China (51361006, 51401059, 51461010, 51361005, 51371060, 51201041, and 51201042), Guangxi University Research Project (YB2014132, 2013ZD023) and Guangxi Natural Science Foundation (2014GXNSFAA118043, 2013GXNSFBA019239, 2013GXNSFBA019034, 2014GXNSFAA118333). This work was partially supported by the Guangxi Collaborative Innovation Center of Structure and Property for New Energy Materials.

Conflicts of Interest

The authors declare no conflict of interest.

References

1. Liu, Y.F.; Pan, H.G.; Gao, M.X.; Wang, Q.D. Advanced hydrogen storage alloys for Ni/MH rechargeable batteries. *J. Mater. Chem.* **2011**, *21*, 4743–4755.
2. Zhao, X.Y.; Ma, L.Q. Recent progress in hydrogen storage alloys for nickel/metal hydride secondary batteries. *Int. J. Hydrogen Energy* **2009**, *34*, 4788–4796.
3. Li, W.; Du, Y.L. Effects of Y Substitution for La on the microstructure and electrochemical properties of $LaNi_{3.55}Mn_{0.4}Al_{0.3}Co_{0.75}$ hydrogen storage alloys. *Mater. Trans.* **2008**, *49*, 2229–2232.
4. Chu, H.L.; Zhang, Y.; Sun, L.X.; Qiu, S.J.; Qi, Y.N.; Xu, F.; Yuan, H.T. Structure and electrochemical properties of composite electrodes synthesized by mechanical milling Ni-free $TiMn_2$-based alloy with La-based alloys. *J. Alloys Compd.* **2007**, *446–447*, 614–619.
5. Tsukahara, M.; Kamiya, T.; Takahashi, K.; Kawabata, A.; Sakurai, S.; Shi, J.; Takeshita, H.T.; Kuriyama, N.; Sakai, T. Hydrogen storage and electrode properties of V-based solid solution type alloys prepared by a thermic process. *J. Electrochem. Soc.* **2000**, *147*, 2941–2944.
6. Zhang, Y.; Chen, L.X.; Lei, Y.Q.; Wang, Q.D. The effect of partial substitution of Ti with Zr, Cr or V in the $Mg_{35}Ti_{10}Ni_{55}$ electrode alloy on its electrochemical performance. *Electrochim. Acta* **2002**, *47*, 1739–1746.

7. Iwakura, C.; Inoue, H.; Furukawa, N.; Nohara, S. Effects of carbon crystallinity on hydriding-dehydriding and charge-discharge characteristics of MgNi alloy–carbon material composites. *Mater. Trans.* **2002**, *43*, 2706–2710.
8. Chen, J.; Kuriyama, N.; Takeshita, H.T.; Tanaka, H.; Sakai, T.; Haruta, M. Hydrogen storage alloys with $PuNi_3$-type structure as metal hydride electrodes. *Electrochem. Solid–State Lett.* **2000**, *3*, 249–252.
9. Qiu, S.J.; Chu, H.L.; Zhang, J.; Zhang, Y.; Sun, L.X.; Xu, F.; Sun, D.L.; Ouyang, L.Z.; Zhu, M.; Grolier, J.P.E.; Frenkel, M. Effect of La partial substitution for Zr on the structural and electrochemical properties of $Ti_{0.17}Zr_{0.08-x}La_xV_{0.35}Cr_{0.1}Ni_{0.3}$ (x = 0–0.04) electrode alloys. *Int. J. Hydrogen Energy* **2009**, *34*, 7246–7252.
10. Kadir, K.; Kuriyama, N.; Sakai, T.; Uehara, I.; Eriksson, L. Structural investigation and hydrogen capacity of $CaMg_2Ni_9$: A new phase in the AB_2C_9 system isostructural with $LaMg_2Ni_9$. *J. Alloys Compd.* **1999**, *284*, 145–154.
11. Kadir, K.; Sakai, T.; Uehara, I. Structural investigation and hydrogen storage capacity of $LaMg_2Ni_9$ and $(La_{0.65}Ca_{0.35})(Mg_{1.32}Ca_{0.68})Ni_9$ of the AB_2C_9 type structure. *J. Alloys Compd.* **2000**, *302*, 112–117.
12. Kadir, K.; Sakai, T.; Uehara, I. Synthesis and structure determination of a new series of hydrogen storage alloys; RMg_2Ni_9 (R=La, Ce, Pr, Nd, Sm and Gd) built from $MgNi_2$ Laves-type layers alternating with AB_5 layers. *J. Alloys Compd.* **1997**, *257*, 115–121.
13. Kadir, K.; Sakai, T.; Uehara, I. Structural investigation and hydrogen capacity of YMg_2Ni_9 and $(Y_{0.5}Ca_{0.5})(MgCa)Ni_9$: New phases in the AB_2C_9 system isostructural with $LaMg_2Ni_9$. *J. Alloys Compd.* **1999**, *287*, 264–270.
14. Kohno, T.; Yoshida, H.; Kawashima, F.; Inaba, T.; Sakai, I.; Yamamoto, M.; Kanda, M. Hydrogen storage properties of new ternary system alloys: La_2MgNi_9, $La_5Mg_2Ni_{23}$, La_3MgNi_{14}. *J. Alloys Compd.* **2000**, *311*, L5–L7.
15. Liu, Y.F.; Cao, Y.H.; Huang, L.; Gao, M.X.; Pan, H.G. Rare earth–Mg–Ni-based hydrogen storage alloys as negative electrode materials for Ni/MH batteries. *J. Alloys Compd.* **2011**, *509*, 675–686.
16. Liu, Y.F.; Pan, H.G.; Gao, M.X.; Zhu, Y.F.; Lei, Y.Q.; Wang, Q.D. The effect of Mn substitution for Ni on the structural and electrochemical properties of $La_{0.7}Mg_{0.3}Ni_{2.55-x}Co_{0.45}Mn_x$ hydrogen storage electrode alloys. *Int. J. Hydrogen Energy* **2004**, *29*, 297–305.
17. Pan, H.G.; Liu, Y.F.; Gao, M.X.; Zhu, Y.F.; Lei, Y.Q.; Wang, Q.D. Electrochemical properties of the $La_{0.7}Mg_{0.3}Ni_{2.65-x}Mn_{0.1}Co_{0.75}Al_x$ ($x = 0–0.5$) hydrogen storage alloy electrodes. *J. Electrochem. Soc.* **2005**, *152*, A326–A332.
18. Wu, J.M.; Li, J.; Zhang, W.P.; Muo, F.J.; Tai, L.C.; Xu, R.G. The study on the hydrogen storage properties of $MmNi_{3.55}Co_{0.75}Mn_{0.7-x}Al_x$ compounds. *J. Alloys Compd.* **1997**, *248*, 180–184.
19. Notten, P.H.L.; Latroche, M.; Percheron-Guegan, A. The Influence of Mn on the crystallography and electrochemistry of nonstoichiometric AB_5-type hydride forming compounds. *J. Electrochem. Soc.* **1999**, *146*, 3181–3189.
20. Chu, H.L.; Zhang, Y.; Qiu, S.J.; Qi, Y.N.; Sun, L.X.; Xu, F.; Wang, Q.; Dong, C. Electrochemical performances of cobalt-free $La_{0.7}Mg_{0.3}Ni_{3.5-x}(MnAl_2)_x$ (x = 0–0.20) hydrogen storage alloy electrodes. *J. Alloys Compd.* **2008**, *457*, 90–96.

21. Zhang, Y.; Lei, Y.Q.; Chen, L.X.; Yuan, J.; Zhang, Z.H.; Wang, Q.D. The effect of partial substitution of Zr for Ti on the electrochemical properties and surface passivation film of $Mg_{35}Ti_{10-x}Zr_xNi_{55}$ (x = 1, 3, 5, 7, 9) electrode alloys. *J. Alloys Compd.* **2002**, *337*, 296–302.
22. Han, S.S.; Lee, Y.L.; Goo, N.H.; Jeong, W.T.; Lee, K.S. Improvement of electrode performances of Mg_2Ni by mechanical alloying. *J. Alloys Compd.* **2002**, *330*, 841–845.
23. TOPAS V4: General Profile and Structure Analysis Software for Powder Diffraction Data. Bruker AXS: Karlsruhe, Germany, 2008.
24. Msika, E.; Latroche, M.; Cuevas, F.; Percheron-Guégan, A. Zr-substitution in $LaNi_5$-type hydride compound by room temperature ball milling. *Mater. Sci. Eng. B* **2004**, *108*, 91–95.
25. Pan, H.G.; Yue, Y.J.; Gao, M.X.; Wu, X.F.; Chen, N.; Lei, Y.Q.; Wang, Q.D. The effect of substitution of Zr for La on the electrochemical properties of $La_{0.7-x}Zr_xMg_{0.3}Ni_{2.45}Mn_{0.1}Co_{0.75}Al_{0.2}$ hydrogen storage electrode alloys. *J. Alloys Compd.* **2005**, *397*, 269–275.
26. Chu, H.L.; Zhang, Y.; Sun, L.X.; Tian, Q.F.; Xu, F.; Zhang, T.; Yuan, H.T. Structures and hydrogen storage properties of $Mg_{45}M_5Co_{50}$ (M = Zr, Ni, Al) ternary alloys by mechanical alloying. *Int. J. Electrochem. Sci.* **2006**, *1*, 47–54.
27. Seo, C.Y.; Choi, S.J.; Choi, J.; Park, C.N.; Lee, J.Y. Effect of V and Zr on the electrochemical properties of La-based AB_5-type metal hydride electrodes. *J. Alloys Compd.* **2003**, *351*, 255–263.
28. Pan, H.G.; Liu, Y.F.; Gao, M.X.; Zhu, Y.F.; Lei, Y.Q. The structural and electrochemical properties of $La_{0.7}Mg_{0.3}(Ni_{0.85}Co_{0.15})_x$ (x = 3.0–5.0) hydrogen storage alloys. *Int. J. Hydrogen Energy* **2003**, *28*, 1219–1228.
29. Chu, H.L.; Qiu, S.J.; Sun, L.X.; Zhang, Y.; Xu, F.; Jiang, T.; Li, W.X.; Zhu, M.; Hu, W.Y. The improved electrochemical properties of novel La–Mg–Ni-based hydrogen storage composites. *Electrochim. Acta* **2007**, *52*, 6700–6706.
30. Monnier, J.; Chen, H.; Joiret, S.; Bourgon, J.; Latroche, M. Identification of a new pseudo-binary hydroxide during calendar corrosion of (La, $Mg)_2Ni_7$-type hydrogen storage alloys for Nickel–Metal Hydride batteries. *J. Power Sources* **2014**, *266*, 162–169.
31. Zhu, Y.F.; Pan, H.G.; Gao, M.X.; Ma, J.X.; Li, S.Q.; Wang, Q.D. The effect of Zr substitution for Ti on the microstructures and electrochemical properties of electrode alloys $Ti_{1-x}Zr_xV_{1.6}Mn_{0.32}Cr_{0.48}Ni_{0.6}$. *Int. J. Hydrogen Energy* **2002**, *27*, 287–293.
32. Kuriyama, N.; Sakai, T.; Miyamura, H.; Uehara, I.; Ishikawa, H.; Iwasaki, T. Electrochemical impedance spectra and deterioration mechanism of metal hydride electrodes. *J. Electrochem. Soc.* **1992**, *139*, L72–L73.
33. Ratnakumar, B.V.; Witham, C.; Bowman, R.C., Jr.; Hightower, A.; Fultz, B. Electrochemical studies on $LaNi_{5-x}Sn_x$ metal hydride alloys. *J. Electrochem. Soc.* **1996**, *143*, 2578–2584.
34. Notten, P.H.L.; Hokkeling, P. Double phase hydride forming compounds: A new class of highly electrocatalytic materials. *J. Electrochem. Soc.* **1991**, *138*, 1877–1885.
35. Niu, H.; Northwood, D.O. Enhanced electrochemical properties of ball-milled Mg_2Ni electrodes. *Int. J. Hydrogen Energy* **2002**, *27*, 69–77.
36. Nishima, T.; Ura, H.; Uchida, I. Determination of chemical diffusion coefficients in metal hydride particles with a microelectrode technique. *J. Electrochem. Soc.* **1997**, *144*, 1273–1277.

37. Zheng, G.; Popov, B.N.; White, R.E. Electrochemical determination of the diffusion coefficient of hydrogen through an $LaNi_{4.25}Al_{0.75}$ electrode in alkaline aqueous solution. *J. Electrochem. Soc.* **1995**, *142*, 2695–2698.